Geomechanics and Engineering, *Vol. 28, No. 1* (*2022*) *11-23*
https://doi.org/10.12989/gae.2022.28.1.011

Numerical response of pile foundations in granular soils subjected to lateral load

Muhammad B. Adeel[1a], Muhammad Aaqib[2b], Usman Pervaiz[3c], Jawad Ur Rehman[3d] and Duhee Park*[3]

[1]*Department of Transportation & Geotechnical Engineering, National University of Sciences and Technology (NUST), Risalpur, 23200, Pakistan*
[2]*Department of Civil Engineering, National University of Technology (NUTECH), Islamabad 44400, Pakistan*
[3]*Department of Civil and Environmental Engineering, Hanyang University, Seoul 04763, Korea*

(*Received February 7, 2021, Revised October 7, 2021, Accepted December 8, 2021*)

Abstract. The response of pile foundations under lateral loads are usually analyzed using beam-on-nonlinear-Winkler-foundation (BNWF) model framework employing various forms of empirically derived p–y curves and p-multipliers. In practice, the p–y curve presented by the American Petroleum Institute (API) is most often utilized for piles in granular soils, although its shortcomings are recognized. The objective of this study is to evaluate the performance of the BNWF model and to quantify the error in the estimated pile response compared to a rigorous numerical model. BNWF analyses are performed using three sets of p–y curves to evaluate reliability of the procedure. The BNWF model outputs are compared with results of 3D nonlinear finite element (FE) analysis, which are validated via field load test measurements. The BNWF model using API p–y curve produces higher load–displacement curve and peak bending moment compared with the results of the FE model, because empirical p–y curve overestimates the stiffness and underestimates ultimate resistance up to a depth equivalent to four times the pile diameter. The BNWF model overestimates the peak bending moment by approximately 20–30% using both the API and Reese curves. The p-multipliers are revealed to be sensitive on the p–y curve used as input. These results highlight a need to develop updated p–y curves and p-multipliers for improved prediction of the pile response under lateral loading.

Keywords: BNWF; finite element; pile; *p*-multiplier; *p–y* curve

1. Introduction

Pile foundations are widely used to support a variety of structures, including tall buildings, long-span bridges, and offshore structures. Estimation of the lateral response is an important component in the design of pile foundations. The methods available to assess the lateral response of a single pile include the elastic solution proposed by Poulos and Davis (1980), strain wedge model proposed by Ashour et al. (1998), and continuum analysis (Muqtadir and Desai 1986, Brown and Shie 1990, Trochanis *et al.* 1991, Yang and Jeremić 2002, Bouzid *et al.* 2013, Qin and Guo 2014, Stacul *et al.* 2020, Xu *et al.* 2020).

The BNWF model is most often used in practice. In the model, the three-dimensional (3D) soil and pile interaction is represented by the *p–y* curve, where *p* is the soil resistance and *y* is the lateral displacement. Thus, this method is also referred to as the *p–y* model. Various forms of *p–y* curves are used for analyzing pile response in granular soil, such as those presented by Reese *et al.* (1974) and the American Petroleum Institute API (2007), hereafter simply denoted as the Reese and API curves, respectively. The Reese curve is one of the earliest equations developed for analyzing piles embedded in granular soil. In practice, the nonlinear API curve, which was developed to fit the Reese functional form, is widely used. Murchison and O'Neill (1984) reported, based on 14 static and 10 slow cyclic tests, that the API curve is not representative of the measurements. Zhang *et al.* (2005) showed that the API recommendation for calculating the ultimate resistance of cohesionless soils underestimates the ultimate lateral resistance at shallow depths but overestimates the ultimate lateral resistance at greater depths. Based on 3D finite element (FE) results, McGann *et al.* (2010) also reported that the maximum stiffness and ultimate soil resistance are both significantly overestimated when the API recommendations are employed for static analysis of a single pile embedded in cohesionless soil. Based on a suite of centrifuge tests, Choi *et al.* (2013) reported that the API curve deviates from the experimentally derived output; the ultimate soil resistance is underestimated, whereas the initial stiffness is overestimated. Fayyazi (2015) used both the 3D finite difference and BNWF model with the API curve. It was revealed that two models provide significantly different outputs, demonstrating that use of the API curve does not provide a reasonable estimate of the pile–soil interaction. Rahmani *et al.* (2018) concluded that the BNWF model with the API curve fails to simulate the pile–soil interaction for both static and dynamic loadings. Although the limitations of the API curve have been

*Corresponding author, Professor
E-mail: dpark@hanyang.ac.kr
[a]Assistant Professor
[b]Assistant Professor
[c]Ph.D.
[d]Ph.D.

ISSN: 2005-307X (Print), 2092-6219 (Online)

highlighted in an extensive number of studies, these curves are still widely employed owing to their ease of use. Instead of the API curve, Rollins *et al.* (2005) used the Reese *p–y* curve for analyzing pile foundations in sands and compared the numerically calculated results with those of lateral load tests. It was reported that the results were satisfactorily in agreement. It is interesting to note that favorable fitting was obtained when the Reese curve was used, whereas misfits with the field measurements were yielded in the case of the BNWF model with the API curve. There is a need to test the predictions using both curves, and examine the causes for the performance variability.

The BNWF model is also widely used to simulate the group pile response under lateral loading. The soil resistance of a group pile is reduced because of the "shadowing effect" and the "edge effect," as reported by Larkela (2008). This reduction in resistance is simulated in the BNWF model via a reduction factor, termed the *p*-multiplier, which was first proposed by Brown *et al.* (1988). A higher value of the *p*-multiplier is applied to the leading row relative to those applied to the trailing rows to account for the shadowing effects. Various studies recommend that *p*-multipliers for squared vertical groups are functions of the center-to-center spacing and the soil type (Brown *et al.* 1988, McVay *et al.* 1995, Ruesta and Townsend 1997, Rollins *et al.* 1998, Rollins *et al.* 2003, Chandrasekaran *et al.* 2009, Adeel *et al.* 2021). Extensive studies have been performed to derive the *p*-multipliers from field and model experiments (Brown *et al.* 1987, Brown *et al.* 1988, Morrison and Reese 1988, McVay *et al.* 1995, Ruesta and Townsend 1997, McVay *et al.* 1998, Rollins *et al.* 1998, Rollins *et al.* 2005, Walsh 2005, Christensen 2006, Rollins *et al.* 2006).

After selection and application of the *p–y* curves throughout the pile length, the *p*-multiplier is derived through an iterative process involving comparisons with the group pile load test measurements. This procedure, although proven to be successful in reproducing the field load–displacement output, presents several inherent limitations. Firstly, the *p*-multiplier determined for a particular set of *p–y* curves may not be applicable for another set of curves. Secondly, most often only the load–displacement response is compared in derivation of the *p*-multiplier, ignoring the bending moment response, which is an important design parameter. The literature review reveals that uncertainties remain in estimations of both the *p–y* curve and *p*-multiplier for pile foundations in granular soils. However, the residual of the output calculated from a BNWF analysis compared with the measurements and a rigorous procedure including the nonlinear FE analysis have not yet been thoroughly examined and quantified. Therefore, it has not been possible for the engineers to estimate the error in the estimated pile response when using the BNWF model.

We performed a series of 3D FE and BNWF analyses to simulate single and group pile lateral load tests. The 3D FE model, validated against the field lateral load test results, is considered as the reference approach. The *p–y* curves extracted for single pile from the FE analysis are compared with the API and Reese curves. The differences between the numerically and empirically derived curves are quantified. The *p*-multipliers are also derived using a suite of *p–y* curves. The sensitivity of the *p*-multiplier on *p–y* functional form is examined. Based on these quantitative assessments, practical guidelines for the selection of *p–y* curves and *p*-multipliers are provided.

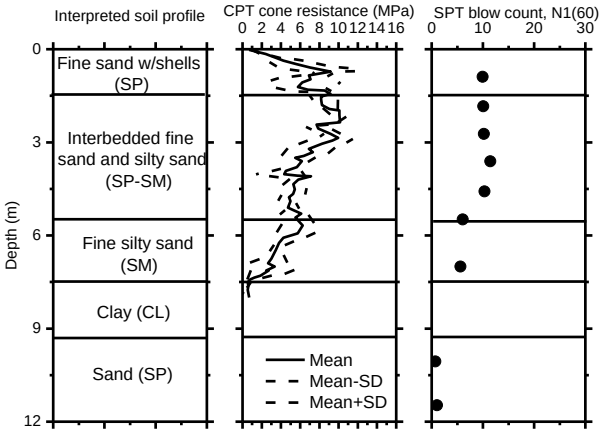

Fig. 1 Site stratigraphy, CPT cone tip resistance, and SPT blow count profiles measured for field pile load tests performed at Treasure Island site (modified after Rollins *et al*. (2005)

2. Reference lateral load tests data

We used the lateral load test measurements reported by Rollins *et al*. (2005) and Walsh (2005) as the reference data to validate the numerical model.

2.1 Rollins et al. (2005)

We used the lateral load test measurements reported by Rollins *et al*. (2005) as the reference data to validate the numerical model. The site profile consists of loose fine sand (SP-SM) overlying silty sand (SM) and Young Bay mud. The in-situ tests performed at the site include cone penetration tests (CPTs), standard penetration tests (SPTs), and geophysical tests. The site stratigraphy and SPT blow count profiles are shown in Fig. 1.

The soil profile consists of a sand deposit that extends to a depth of 7.49 m underlain by soft clay. The water table was measured to be 0.5 m below the surface for the single pile test, whereas it rose to 0.1 m below the surface when the group pile test was performed. The depth below the excavated ground was 11.84 m.

Single and group pile field tests were performed using steel piles with an outer diameter (D) of 0.324 m and a wall thickness (t) of 9.5 mm. The embedded length of the pile was approximately 11.5 m, and the pile was driven open-ended. The moment of inertia of a pile section was 1.16×10^8 mm^4; however, an angle iron was attached to opposite sides of the pile in the direction of loading, which increased the moment of inertia to 1.43×10^8 mm^4. Pile heads were horizontally pushed up to 38 mm via jacking system placed 0.69 m and 0.86 m above the ground surface for single and

Table 1 Soil properties used in numerical simulations

Layer Thickness (m)	Soil type	Effective Unit weight (kN/m^3)	Cohesion (kPa)	Friction Angle (ϕ°)	h	m	r	H_o
1.4	Sand	14.9	0	39	0.0026	1.42	0.02	0.001
4.1	Sand	10.3	0	38	0.0177	1.0097	0.04	0.001
1.99	Sand	10.3	0	36	0.0189	1.008	0.05	0.042
1.71	Soft Clay	9.5	19.5	0	0.0187	0.9999	0.04	0.014
2.64	Sand	10.3	0	34	0.0195	1.0036	0.1	0.254

Table 2 Soil properties used in numerical simulations

Layer Thickness (m)	Soil type	Effective Unit weight (kN/m^3)	s_u (kPa)	Friction Angle (ϕ°)	h	m	r	H_o
2.4	Sand	16.7	-	48	0.0015	1.78	0.04	0.001
0.3	Clay	16.7	41	-	0.0154	1.15	0.11	0.001
1	Clay	16.7	50	-	0.0127	1.3	0.13	0.001
0.9	Clay	16.7	40	-	0.0106	1.244	0.09	0.001
1.7	Sand	19.1	-	38	0.0081	0.31	0.08	0.001
1.7	Clay	19.1	57	-	0.0096	1.49	0.16	0.001
4.8	Sand	19.1	-	33	0.013	1.19	0.102	0.001

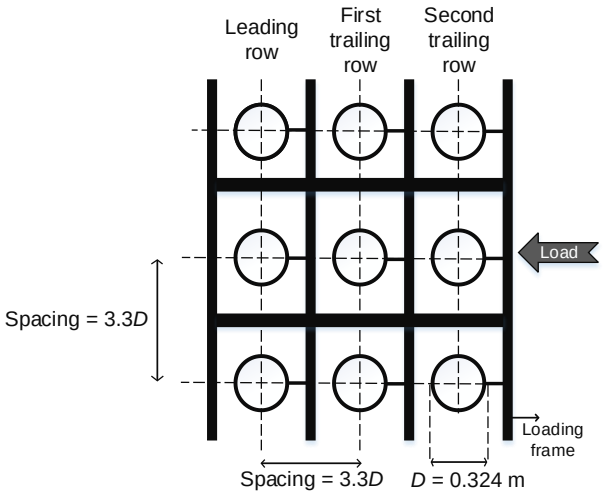

Fig. 2 Plan view of 3 × 3 group pile load test of Rollins *et al.* (2005)

group piles, respectively. For the group pile test, the piles were driven in a 3 × 3 square pattern with a pile center-to-center spacing of 3.3*D*. A plan view of the group pile test is shown Fig. 2.

The measured shear wave velocity was not been presented in the paper of Rollins *et al*. (2005). However, the average shear wave velocity in the upper 6 m was reported to be approximately 120 m/s. Because the shear wave velocity profile was unavailable, we calculated it using the correlation proposed by Kwak *et al.* (2015) as follows

$$ln(V_s)_{ij} = (\beta_0)_{SG,N} + (\beta_1)_{SG,N} ln(N_{60})_{ij} + (\beta_2)_{SG,N} ln(\sigma_v')_{ij} \quad (1)$$

where $(\beta_0)_{SG,N}$, $(\beta_1)_{SG,N}$, and $(\beta_2)_{SG,N}$ are regression coefficients that depend on the soil type and range of SPT blow counts; *i* and *j* are the site index and layer index, respectively; and σ_v' is the vertical effective stress. The $N_{1(60)}$ blow count was converted to N_{60} using the following Eq.

$$(N_1)_{60} = \left(\frac{P_a}{\sigma_v'}\right)^n N_{60} \quad (2)$$

Because of the unavailability of SPT measurements in the clay layer, V_s for the clay layer was determined from the CPT measurements using the following empirical correlation proposed by Mayne and Rix (1995)

$$V_s = 1.75 (q_c)^{0.627} \quad (3)$$

where V_s is the shear wave velocity, and q_c is the cone tip resistance (kPa).

The V_s profile is shown in Fig. 3. The soil properties employed in the numerical simulations were those used in the study of Rollins *et al*. (2005), which include the unit weight, friction angle of the sand layers, and undrained cohesion of the clay layer. These properties are summarized in Table 1.

2.2 Walsh (2005)

Another test used to validate the FE model is pile test performed by Walsh (2005). The testing program included a full scale 3x5 pile group subjected to lateral loading. Fig. 4 shows a full scale 3x5 pile group. Steel tube piles with an outer diameter of D=0.324 m and a thickness of 0.0095 m were used. The piles were spaced at a distance of 3.92D

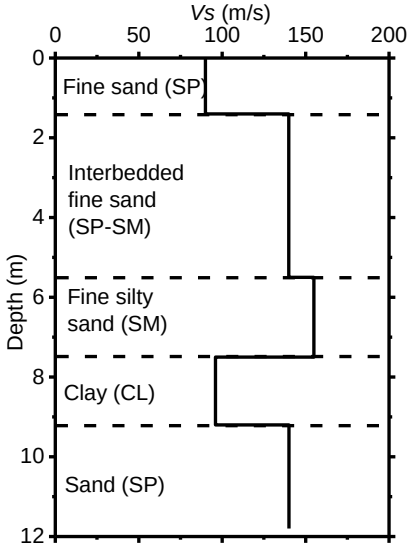

Fig. 3 V_s profile used in the FE model

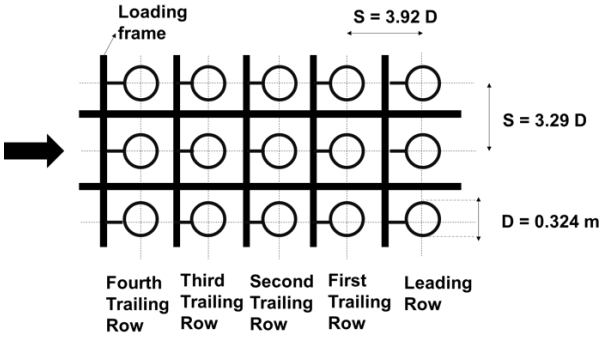

Fig. 4 Plan view of 3 × 5 group pile load test of Walsh (2005)

(1.27 m) in the direction of loading. The pile spacing was 3.29D (1.07 m) perpendicular to the loading direction. The piles had an embedded length of 12.8 m. The water table was at a depth of 2.1 m. The pile heads were horizontally loaded predetermined pile head deflections at a height of 0.48 m above the ground level, simulating a free pile head condition.

The field and soil tests performed are documented in Walsh (2005). The soil properties determined in Walsh (2005) were used in the simulation. Because the shear wave velocity profile was unavailable, we calculated it using the correlation proposed by Kwak *et al*. (2015). $N_{1(60)}$ blow count was converted to N_{60} using the Eq. (2). Because of the unavailability of SPT measurements in the clay layer, V_s for the clay layer was determined from the undrained shear strength (s_u) provided in Walsh (2005) using the following empirical correlation proposed by Dickenson (1994)

$$V_s(m/s) = \ 23 \ s_u^{0.475} \tag{4}$$

where s_u is the undrained shear strength with a unit of kPa. The V_s and SPT profiles are shown in Fig. 5. The soil properties employed in the numerical simulations were those used in the study of Walsh (2005). These properties are summarized in Table 2.

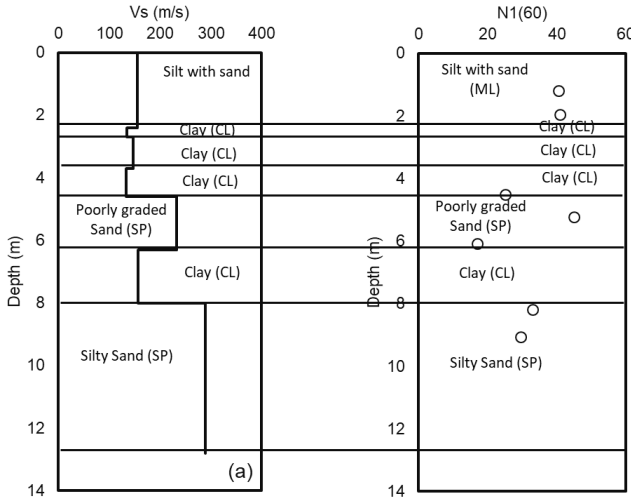

Fig. 5 Site stratigraphy showing (a) Vs profile (b) SPT blow count profiles

3. Numerical model

Both the FE and BNWF models were used to simulate single and group pile foundations subjected to lateral loading. The details of both models are presented in the following section.

3.1 FE model (Rollins et al. 2005)

We used the commercial finite element analysis program Abaqus (2017) to simulate the pile-soil interaction. The 3D nonlinear computational model for the group pile test is shown in Fig. 6.

The convergence analysis for the finite element mesh was also performed such that the to determine optimum element sizes to obtain accurate results. Additionally, a sensitivity analysis was performed to confirm that the boundaries do not influence the calculated pile response. The mesh was generated in such a way that it is finer near the piles and coarser towards the boundaries of the computational domain. The width of the smallest element was 0.15*D*. The size of the computational domain was determined after a sensitivity analysis such that the calculated responses are not affected by the boundaries. The length and width of the computational model are 10 m and 5 m, respectively, whereas the depth of the model is 11.84 m. Eight-node brick elements were used to model both the piles and soil. The mesh of the numerical models for single pile and pile group consists of 26454 and 32328 elements, respectively. The mesh was generated such that the element size gradually decreases in the direction toward the pile.

The interface between the piles and soil was modeled using a surface-to-surface contact model that allows for both slipping and normal separation (gapping). The Coulomb model was used to simulate the tangential slip, considering a friction coefficient of $\tan(2/3\phi)$ for the sand layer, as used in the study of Park et al. (2016). For the clay layer, the friction coefficient was set to unity using the equation proposed by Sladen (1992).

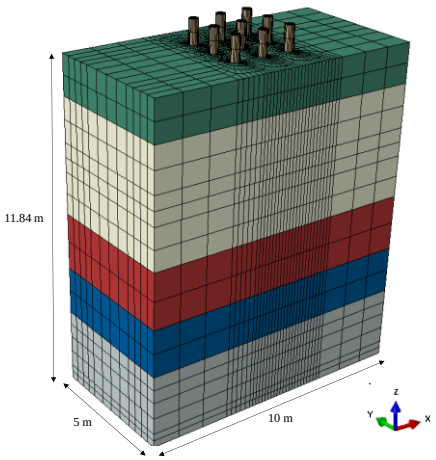

Fig. 6 Finite element model of 3 × 3 group pile foundation

The bottoms of the piles were tied to the soil elements. The bottom of the computational domain was fixed in both horizontal and vertical directions. The horizontal displacement constraints were applied at the lateral boundaries. No constraint was applied at the surface of the soil domain.

The piles were modeled as solid rods with the same outer diameters as those of the steel piles used in the lateral load tests. Because of this difference in the section of the pile used, the modulus of elasticity, E, of the pile elements was adjusted such that the resulting flexural rigidity is identical to that of the steel pile. The properties of the steel pile employed in the numerical simulations are listed in Table 1. The bending moment along the pile was extracted from the solid elements using the free body cut option under View cut manager in ODB file in Abaqus, which automatically calculates the bending moment from the normal stresses on the cross-section.

The bounding surface plasticity soil model proposed by Borja and Amies (1994) was adopted to simulate the nonlinear behavior of the soil. The shear modulus reduction curve derived from the model can be expressed as follows

$$\frac{G}{G_{max}} = 1 - \frac{3}{2\gamma_0}\int_0^{2\tau_0}\left[h\left(\frac{R/\sqrt{2}+\tau_0-\tau}{\tau}\right)^m + H_0\right]^{-1} d\tau \qquad (5)$$

where $\frac{G}{G_{max}}$ is the secant shear modulus normalized to the maximum shear modulus; γ_0 is the shear strain; τ_0 is the shear stress; R is the radius of the bounding surface; h and m are the coefficient and exponent of the exponential hardening function, respectively; and H_o is the kinematic hardening parameter. This equation was used to calibrate the soil parameters. The plasticity model was developed into a UMAT subroutine code for Abaqus by Zhang *et al.* (2017), who also developed an associated code for selecting the input parameters automatically. Both the subroutine and the input parameter selection code developed by Zhang *et al.* (2017) were used in the numerical simulations in this study.

The shear modulus reduction curves of Darendeli (2001) were used as the reference data to fit the nonlinear model.

Table 1 Properties of the steel piles Rollins *et al*. (2005)

Parameter	Value
Pile Type	Steel pipe pile ASTM A252 Grade 3
Diameter (m)	0.324
Thickness (m)	0.0095
Moment of inertia (mm^4)	1.43×10^8
Equivalent modulus of elasticity, E (Gpa)	53

The plasticity index for the clay layer was set to 20 based on the in-situ tests conducted by Ferritto (1993). Because the shear modulus reduction curves in their original forms are known to not match the shear strength, the generalized quadratic/hyperbolic (GQ/H) constitutive model (Groholski *et al*. 2016) was used to apply the shear strength correction. The Mohr–Coulomb failure criterion was used to calculate the shear strength of the sands, the friction angle of which are listed in Table 1. For the clay layer, the measured undrained shear strengths presented in Rollins *et al*. (2005) were used. Fig. 8 compares the target and numerically calculated curves for all soil layers. The nonlinear soil model is shown to fit the target curves favorably.

The lateral resistance (p) for the p–y curve was calculated via double derivation of the bending moment as follows

$$p = \frac{d^2M(z)}{dz^2} \qquad (6)$$

where $M(z)$ is the bending moment of the pile at depth z. The bending moment along the pile was fitted with a seventh-order polynomial function, as recommended by Brandenberg *et al*. (2010). The lateral displacement (y) of the pile was extracted directly from the FE analysis.

3.2 FE model (Walsh 2005)

The 3D nonlinear computational model for the group pile test is depicted in Fig. 7. The convergence and sensitivity analysis for the finite element mesh was performed in line with the previous case study. The width of the smallest element was 0.1D. The length and width of the computational model were 12 m and 8 m, respectively, whereas the depth of the model was 12.8 m. Eight-node brick elements were used to model both the piles and soil. The mesh of the numerical models for single pile and pile group consists of 45931 and 394036 elements, respectively. The mesh was created in such a way that the element size steadily reduces as it approaches the pile.

A surface-to-surface contact model was used to simulate the interface between the piles and the soil, which allows for both slippage and normal separation. The soil elements were connected to the bottoms of the piles. In both horizontal and vertical directions, the bottom of the computational domain was fixed. At the lateral boundaries, horizontal displacement constraints were applied. At the soil domain's surface, no constraint was applied. The piles were

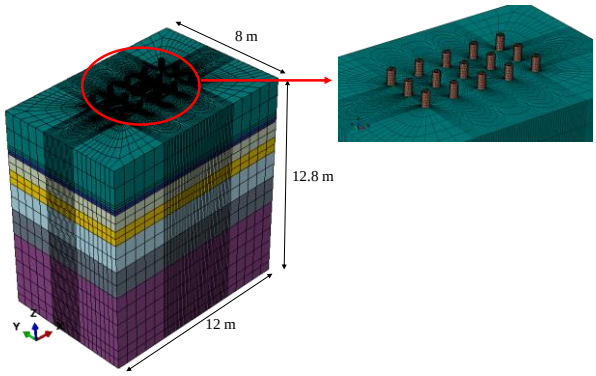

Fig. 7 Finite element model of 3×5 group file foundation

Table 2 Properties of the steel piles Walsh (2005)

Parameter	Value
Pile Type	Steel pipe pile ASTM A252 Grade 3
Diameter (m)	0.324
Thickness (m)	0.0095
Moment of inertia (mm^4)	1.43×10^8
Equivalent modulus of elasticity, E (Gpa)	53

modelled as solid rods with outer diameters that matched the steel piles utilized in the lateral load tests. Table 2 lists the parameters of the steel piles used in the numerical simulations.

Borja and Amies (1994) bounding surface plasticity soil model was used to replicate the soil's nonlinear behavior. The properties of soil layers used in the numerical model are listed in Table 2.

3.3 BNWF model

We also used the BNWF model to simulate the lateral load tests and compare the results of the FE model. The commercial software packages LPILE version 5.0.27 (Reese *et al.* 2004) and GROUP version 8.0.9 (Reese *et al.* 1996) were used. Both LPILE and GROUP are widely used in practice (Rollins *et al.* 2005, Walsh 2005, Rollins *et al.* 2006, Fayyazi *et al.* 2014). For the sand layers, the *p–y* curves recommended by Reese *et al.* (1974) and API (2007) were used, the functional forms of which are presented in detail in the following paragraph. The *p–y* curve proposed by Matlock (1970) was used for the clay layer. For the BNWF mode the free-head condition was applied to the pile head. For the pile tip, both the lateral and axial displacements were fixed, whereas the rotation was allowed.

The Reese *p–y* curve is composed of four sets of curves, including three linear lines and a parabola, as shown in Fig. 9. The parameters D and z in Fig. 9 represent the diameter of the pile and depth from the ground surface, respectively. The initial linear portion of the *p–y* curve up to y_k represents the elastic behavior of sand. Representative values for k_{py} are provided in a tabular form in Reese *et al.* (1974) and also listed in Table 5.

The linear curve portion is followed by a parabola up to a displacement of $y_m = D/60$ and pressure of p_m. This parabola is followed by another sloping linear curve up to $y_u = 3D/80$, at which the ultimate resistance, p_u, is reached. The response becomes perfectly plastic at this state. Both p_m and p_u are functions of p_{ct}, which is defined as the ultimate resistance near the ground surface and is calculated as follows

$$p_{ct}=\gamma z\left[\frac{K_o H\tan\varphi\sin\beta}{\tan(\beta-\varphi)\cos\alpha}+\frac{\tan\beta}{\tan(\beta-\alpha)}(D+z\tan\beta\tan\alpha)\right.$$
$$\left.+K_o z\tan\beta(\tan\varphi\sin\beta-\tan\alpha)-K_a D\right] \quad (7)$$

where $\alpha=\frac{\varphi}{2}$, $\beta=45+\frac{\varphi}{2}$, $K_o=0.4$, $K_a=\tan^2(45-\frac{\varphi}{2})$, and γ is the submerged unit weight; p_m and p_u are calculated as Bp_{ct} and Ap_{ct}, respectively, where A and B are curve-fitting parameters that are functions of the normalized depth, z/D. Charts (not shown in this study) were provided to determine parameters A and B for both static and cyclic loading conditions.

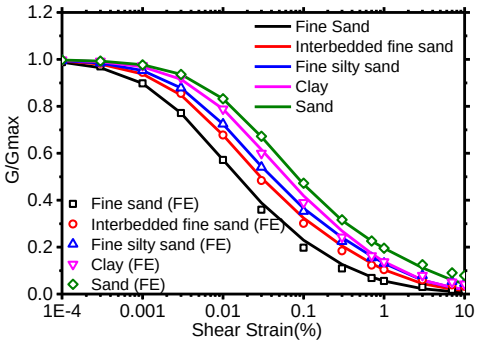

Fig. 8 Comparison of target nonlinear curves and normalized shear modulus reduction curves for selected soil layers from FE model

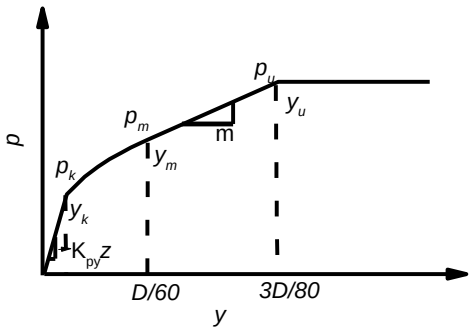

Fig. 9 *p–y* curve proposed by Reese *et al.* (1974)

Table 5 Initial stiffness (kpy) values proposed by Reese *et al.* (1974)

	Relative density		
	Loose	Medium	Dense
k_{py} (MN/m^3) (Below water table)	5.4	16.3	34
k_{py} (MN/m^3) (Above water table)	6.8	24.4	61

$$p = Ap_{ct}\, tanh\left(\frac{k_{py}zy}{Ap_{ct}}\right) \quad (8)$$

The initial stiffness is k_{py} and the ultimate resistance is Ap_{ct}, both of which are identical to those of the Reese curve. However, the definition of k_{py}, p_{ct}, and A are different. A figure dependent on the friction angle and relative density was provided to determine k_{py}, whereas the following equation replaces Eq. (7) for p_{ct}:

$$p_{ct}=(C_1z+C_2D)\gamma z \quad (9)$$

where C_1 and C_2 are ϕ-dependent coefficients, selected from the charts provided by the API, and A is defined as $\left(3\text{-}0.8\frac{z}{D}\right)\geq 0.9$. Although dissimilar in form, the values of the three parameters listed above are only marginally different from those presented in Reese**.**

The API curve is most often applied in practice owing to its ease of use. Fig. 11 compares the Reese and API curves for ϕ = 39° at $z = D$ = 0.324 m. A pronounced discrepancy is apparent for y from y_k to y_u, where the API curve shows higher resistance than that calculated by the Reese curve.

4. Validation of 3D FE model

The computed responses from the 3D FE analysis for Rollins *et al.* (2005) are shown in Figs. 12-14. Fig. 14 show the comparison of bending moments with measurements of a center pile for leading, first trailing and second tailing row at various displacement levels. The numerical simulations are compared to the measured responses reported in Walsh (2005) in Figs. 15 and 16.

These comparisons between the simulated outputs with the measurement results demonstrate the goodness of the fit. The results reveal that the nonlinear soil model developed by Borja and Amies (1994) can capture the responses of pile groups under lateral loads effectively and that the 3D nonlinear FE model simulates the soil–pile interaction accurately. The FE model is considered as the reference approach in this study. The validated model is used to further probe the soil and pile responses, the results of which are compared with the BNWF model outputs. The details of these analysis are presented in the following section.

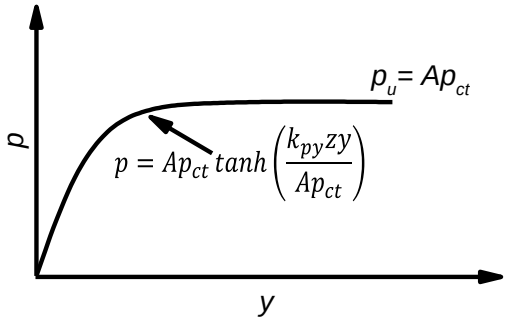

Fig. 1 *p–y* curve proposed by API (2007)

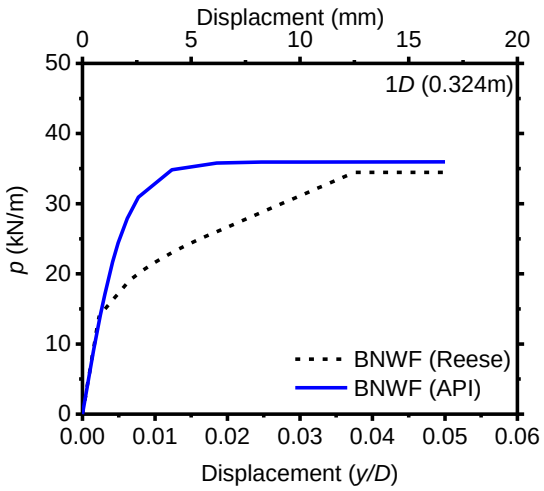

Fig. 11 Comparison of Reese *et al.* (1974) and API (2007) *p–y* curves

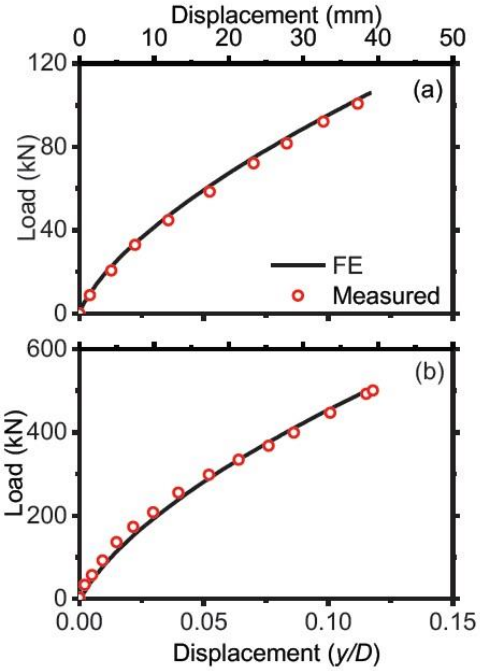

Fig. 12 Comparison of measured (Rollins *et al.* 2005) and calculated total load deflection curves: (a) single pile and (b) 3 × 3 group pile

5. Single pile simulation results

In this section, the outputs obtained from the numerical simulations of the single pile load test are examined. It should be noted that the site profile and configuration of Rollins *et al.* (2005) test were used. The results of the BNWF model incorporating both the Reese and API curves are compared with the FE model outputs. Whereas the field load test was only performed up to y = 38 mm, the pile was further pushed to y = 88 mm in the numerical analysis. Fig. 17 compares the measured load–displacement curves with the computed results.

The load–displacement curve computed by the BNWF model with Reese curve compares favorably with both the

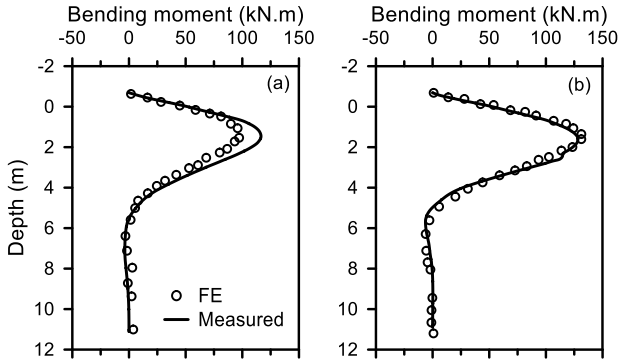

(a) single pile at y = 23 mm (b) single pile at y = 28 mm

Fig. 13 Comparison of measured (Rollins *et al*. 2005) and calculated bending moment profiles of single pile

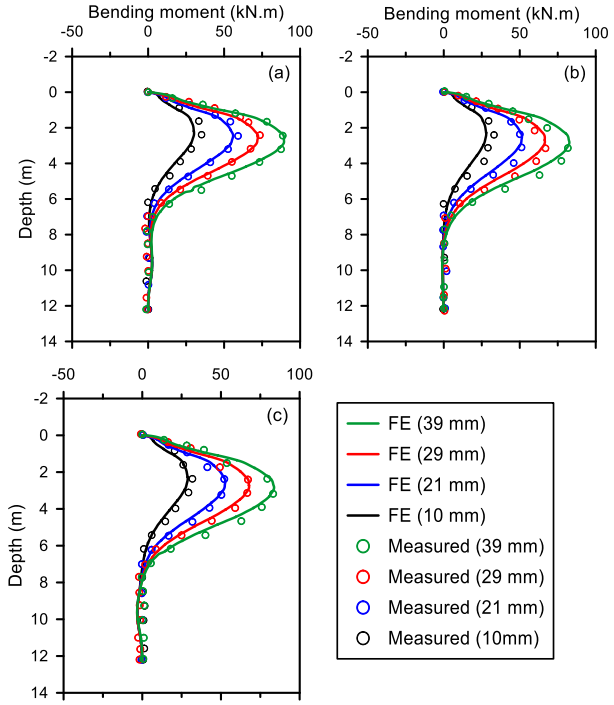

Fig. 14 Comparison of measured bending moment profiles for the center pile (Rollins *et al.* 2005) with those calculated using FE at y = 39, 29, 21 and 10 mm for (a) leading row, (b) first trailing row and (c) second trailing row

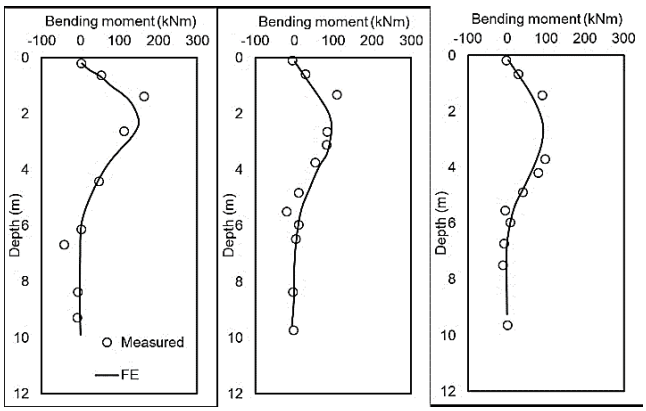

Fig. 15 Computed and measured bending moment (Walsh 2005) of center pile at y = 38 mm: (a) leading row, (b) first trailing row, and (c) fourth trailing row test

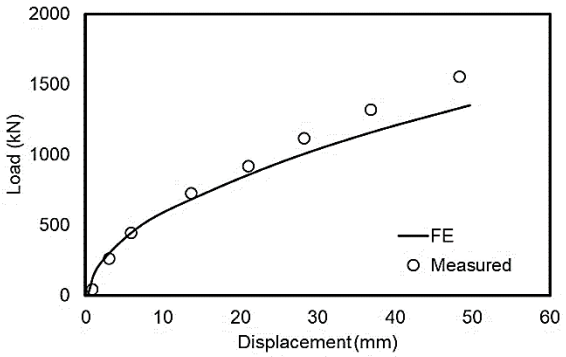

Fig. 16 Computed and measured total load-displacement curve for the test of Walsh (2005)

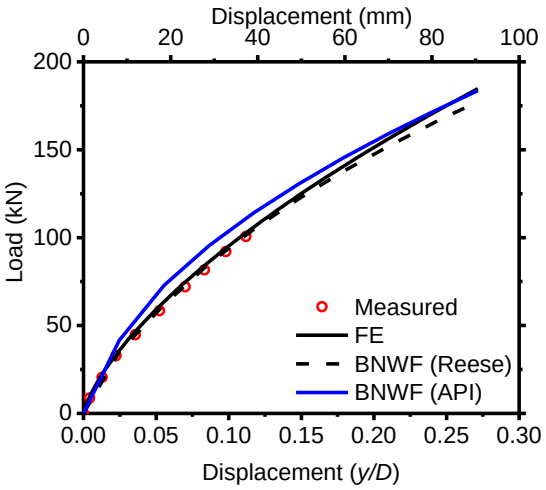

Fig. 17 Comparison of measured load–displacement curve and outputs calculated using FE and BNWF models with Reese *et al.* (1974) and API (2007) curves

measurement and FE model output for y up to 28 mm, but diverges at y = 40 mm, beyond which the FE model produces a stiffer curve. The BNWF model with the API curve significantly overestimates the load–displacement curve. This overestimation may lead to an unconservative design, because the higher estimate of the stiffness is associated with overprediction of the lateral capacity. A comparison of the bending moments, illustrated in Fig. 18, reveals that for y = 28 mm, the moment yielded by the BNWF model with the Reese curve matches reasonably with the peak moment that occurs at a depth of 5 z/D. The BNWF - API model produces a higher peak moment. The residual between the peak moment calculated by the reference analysis and the BNWF model elevates for y = 88 mm, demonstrating that the accuracy is dependent on y.

The relative errors of the calculated loads and moments, which represents the residual between the results of the reference FE model and BNWF analysis method, are shown in Fig. 19. The relative error of the estimated load by the BNWF - Reese model is extremely low, ranging from -0.01 to -0.04, revealing an excellent fit with the FE model. The relative error is higher for the BNWF - API model, peaking at 0.16 for y = 8 mm and decreasing with increasing y. The

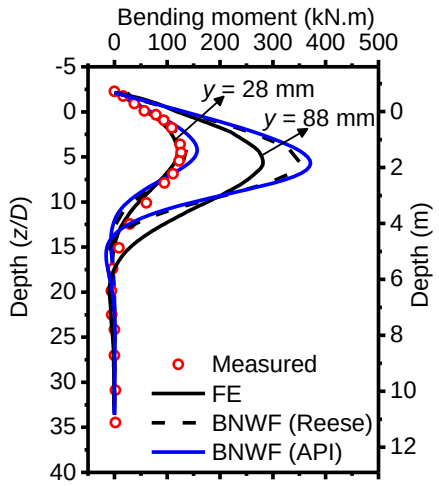

Fig. 18 Comparison of measured bending moments for a single pile with those calculated using FE and BNWF models at y = 28 and 88 mm

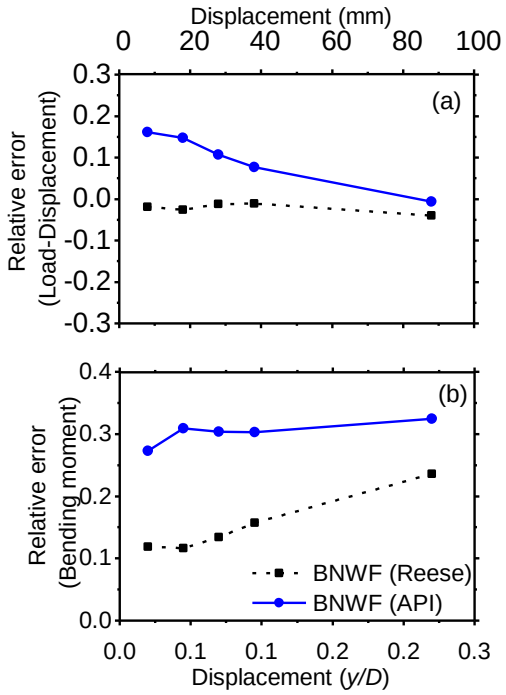

Fig. 19 Relative error between outputs of BNWF and FE models: (a) lateral load and (b) peak bending moment

trend of the relative error in the estimated moment is opposite to that for the load. It is shown to grow with increasing y for the BNWF - Reese model. The relative error increases from 0.11 at y = 8 mm to 0.23 at y = 88 mm.

The p–y curves were extracted from the FE model at selected depths below the ground level and compared with both the Reese and API curves, as shown in Fig. 20. The curves derived from the FE model are shown to yield the lowest stiffness at all depths and highest ultimate strength up to a depth of 4D from the ground level. The ultimate resistance is not mobilized in the FE model, and the resistance is shown to grow with increase in y, except at the

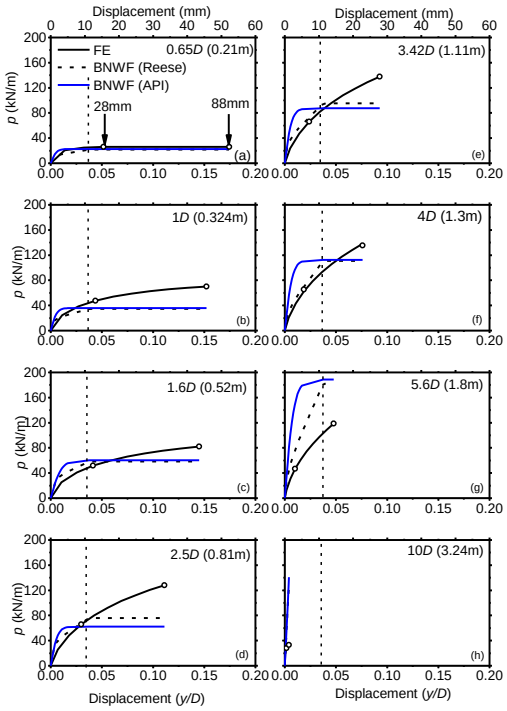

Fig. 20 Comparison of p–y curves extracted from FE model with Reese *et al*. (1974) and API (2007) curves at selected depths: (a) 0.65D, (b) 1D, (c) 1.6D, (d) 2.5D, (e) 3.42D, (f) 4D, (g) 5.6D, and (h) 10D

shallowest depth. This continued grow of the resistance is caused by increment of the shear strength of granular soil with increasing loading. This characteristic is not captured in the empirical p–y curve.

The Reese curves demonstrate a reasonable fit with the FE curves at y up to y_u and to a depth of 4D, whereas the API curves significantly overestimate the resistance in this range. Both curves significantly underestimate the ultimate resistance at depths up to 4D, beyond which they overestimate it. The comparison of the p–y curves provides insight into the computed relative errors between the FE and BNWF models. The BNWF - Reese model provides a good estimate of the load and bending moment up to y = 28 mm because of the similarity in the shape of the p–y curve. The BNWF - API model yields a significantly higher load and peak moment owing to its pronounced overestimation of the resistance at small displacements.

The soil resistance of both the BNWF - Reese and API models dramatically increases at $z > 4D$, inducing a corresponding strong contrast in the resistance at this depth range. This is likely to have resulted in a steeper slope in the lateral displacement profile and a larger moment. The relative error in the calculated moment is shown to grow with increasing y, as plotted in Fig. 14. Lower ultimate resistances for both empirical p–y curves at $z/D < 4$ produce a higher level of deformation within this depth range, whereas significantly higher stiffness at $z/D > 4$ induces lower levels of displacement at this zone. It should also be noted that because p_u of the Reese and API curves are identical, the relative error converges at large y.

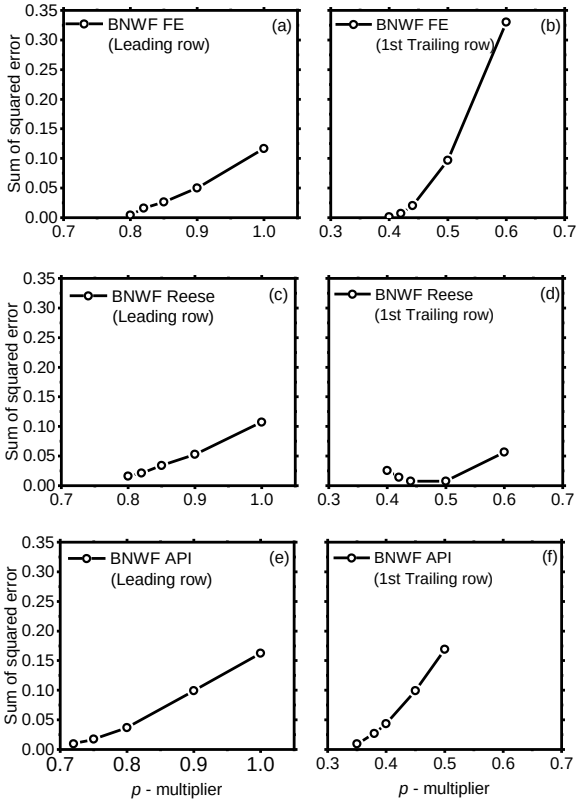

Fig. 21 Variation in sum of the squared error of loads calculated using FE and BNWF models with p-multiplier: (a)-(b) FE curve for leading and first trailing rows, (c)-(d) Reese *et al.* (1974) curve for leading and first trailing rows, (e)-(f) API (2007) curve for leading and first trailing rows

The probing of the soil response provides valuable insight on the sources of the relative error of the BNWF analysis approach compared with the reference model. Based on these numerical simulations, the Reese curve is recommended for use in the BNWF model instead of the API curve. It should also be noted that although the BNWF - Reese model produces better fits with the reference model output, it still provides a conservative estimate of the peak moment.

6. Group pile simulation results

In this section, the numerical simulation outputs of the group pile lateral load test are compared. Again, the site profile and configuration of Rollins *et al.* (2005) test were used. We used three types of curves for the BNWF model: 1) a curve extracted from the single pile FE model (denoted as the FE curve hereafter), 2) Reese curve, and 3) API curve. A consistent difference of approximately 10% between the pressures at the middle and side piles were observed in the numerical simulations. All responses presented hereafter are averaged for a given row. The averaged bending moments and soil resistance (p) for first and second trailing rows were shown to be similar. Therefore, only the results for the first trailing row are displayed hereafter.

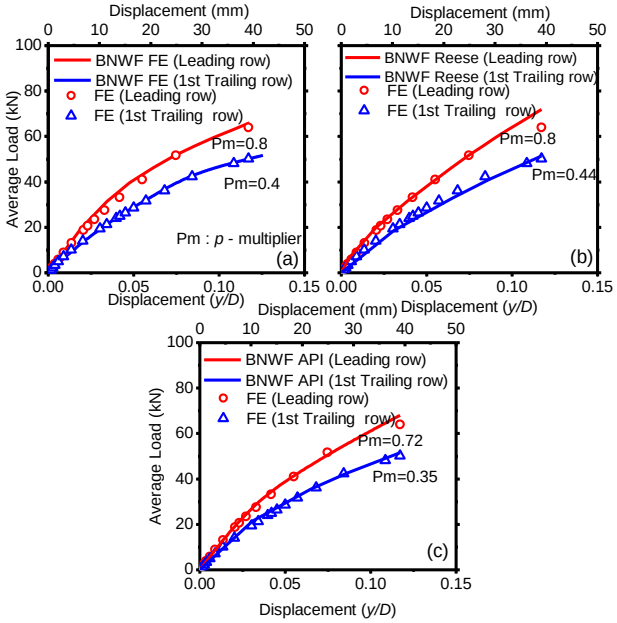

Fig. 22 Comparison of averaged load–displacement curves calculated using FE and BNWF models with three types of p–y curves to simulate the group pile load test: (a) BNWF FE, (b) Reese *et al.* (1974) and (c) API (2007)

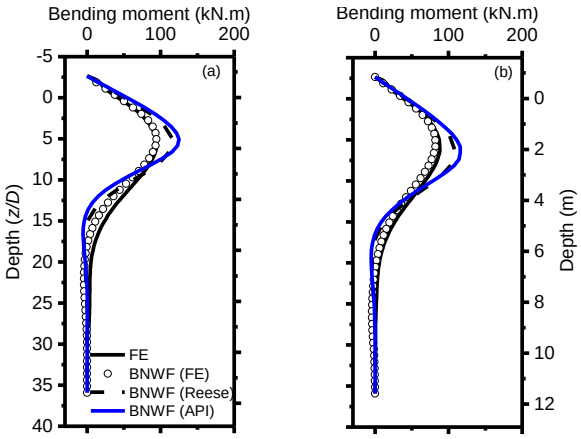

(a) leading row (b) first trailing row

Fig, 23 Comparison of averaged bending moment profiles calculated at y = 38 mm using FE and BNWF models with three types of p–y curves to simulate the group pile load test

The p-multiplier was determined as the value yielding the lowest sum of squared error between the BNWF model computation and the reference load–displacement output, as shown in Fig. 21.

Fig. 22 compares the reference load–displacement curve with the outputs from the BNWF model. The results illustrate that the p-multiplier is dependent on the type of p–y curve used. For the FE curve, p-multipliers of 0.8 and 0.4 corresponding to the leading and first trailing rows, respectively, yield the lowest error. The p-multiplier for the first trailing row increases to 0.44 for the BNWF - Reese model. Both the p-multipliers for the leading and trailing rows decrease to 0.72 and 0.35 for the BNWF - API model,

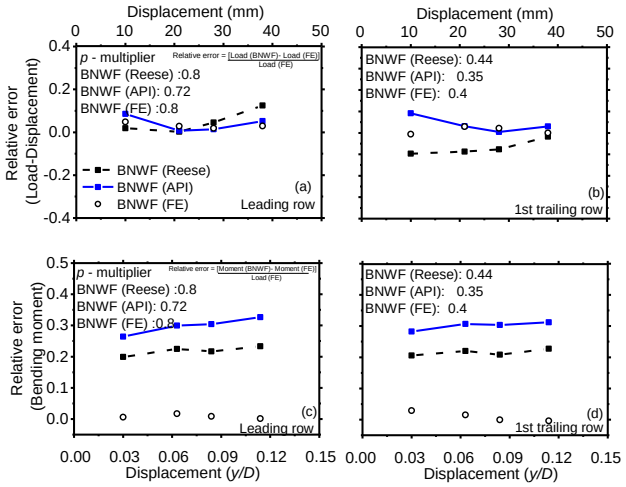

Fig. 24 Relative error between outputs of BNWF and FE models for leading and first trailing rows: (a)-(b) lateral load for leading and first trailing rows, (c)-(d) peak bending moment for leading and first trailing rows

respectively. When the trial-and-error based *p*-multipliers are employed, the outputs of all the BNWF models demonstrate good fits with the reference data.

The evolution of the load and bending moment relative error with displacement are calculated and compared in Fig. 24. A positive error denotes an overprediction of the BNWF model, whereas a negative error represents an underprediction. The relative error for the lateral load of the leading row are shown to be within 0.1. The BNWF - API model over predicts the load at low y and yields a good match at $y > 30$ mm. The BNWF -API model also produces the highest positive error at low y for the trailing row. The relative error of the BNWF -Reese model is lower at low y for the leading row. Overall, the relative error of the load is not significant for both the BNWF models. The error of the peak bending moment, however, is shown to be higher.

The error calculated via the BNWF - API model is shown to increase proportionally with increasing y, reaching 0.32. The BNWF - Reese model produces smaller error that do not exceed 0.23. The BNWF - FE model provides accurate predictions of both the load and peak moment. These comparisons again demonstrate that the BNWF - Reese model provides a more reliable prediction of the load and peak moment than that of the BNWF - API model. Therefore, its use is recommended in design practice in the absence of a curve derived from an FE model.

7. Conclusions

We examine the reliability of the BNWF model and the widely used empirical *p*–*y* curve/*p*-multiplier pairs to predict the responses of single and group piles in granular soil subjected to a lateral load. The *p*–*y* curves used include the empirical functions presented by Reese *et al.* (1974) and (API 2007). The performances of the BNWF models are evaluated through comparison of their results with 3D FE analysis outputs in the form of the relative error. The nonlinear FE model is considered as the reference analysis method, because comparisons with the field load test measurements demonstrate remarkable fits with both the recorded load–displacement curve and bending moment profile. The nonlinear *p*–*y* curves were extracted from the FE model along with the *p*-multiplier. In the case of the pile group, both the pile response and the p-multipliers are compared. The p-multipliers that yield the lowest sum of squared error between the BNWF model output and the reference load–displacement output were selected by trial-and-error. The findings of the study are the following.

- For the single pile, comparisons with the *p*–*y* curves derived from the FE model demonstrate that the Reese *p*–*y* curves produce reasonable fitting at small y, whereas the API curves significantly overestimate the initial stiffness at $z/D < 5$. Both empirical curves are revealed to underestimate the ultimate resistance at $z/D < 5$ and significantly overestimate the soil resistance at higher z/D. The comparisons highlight that the use of Reese curves is recommended over the widely used API curves.
- The relative error shows that the BNWF - Reese model outperforms the BNWF - API model, where the API overpredicts both the load and bending moment. The stiffer estimate of the load-displacement curve using the API curve may lead to an unconservative design, because it is associated with overprediction of the lateral capacity. Therefore, the Reese curves are recommended over the API curves for use in practice.
- The comparisons of *p*-multipliers reveal their sensitivity on the *p*–*y* curve. The *p*-multipliers for the leading and trailing rows for the BNWF - FE model are shown to be in close agreement with those for the BNWF model with Reese curves. However, the *p*-multipliers for the BNWF - API model are demonstrated to be lower in value. This sensitivity analysis demonstrates that a prediction of the *p*–*y* curve should be preceded to the development of the *p*-multiplier.
- The BNWF models using both the Reese and API curves produce 20–30% larger peak bending moments relative to those of the reference output. This relative error in the bending moment is caused by the misfit of the empirical *p*–*y* curve.
- The relative error becomes close to zero when the FE curves are used, again revealing the importance of using reliable *p*–*y* curves.

Acknowledgments

This research was supported by the project titled 'Development and demonstration of a decommission device for piles in shallow sea following international specifications', funded by the Ministry of Oceans and Fisheries, Korea and the Basic Science Research Program through the National Research Foundation of Korea (NRF) funded by the Ministry of Science, ICT and Future Planning [NRF- 201900000000551].

References

Abaqus, S. (2017), *ABAQUS/Standard User's Manual, Version 2017*, Providence, RI: Simulia

Adeel, M.B., Jan, M.A., Aaqib, M. and Park, D. (2021), "Development of simulation based p-multipliers for laterally loaded pile groups in granular soil using 3D nonlinear finite element model", *Appl. Sci.*, **11**(1), 26. https://doi.org/10.3390/app11010026.

API (2007), *Recommended practice for planning, designing, and constructing fixed offshore platforms. API Recommended Practice 2A-WSD. 21st Ed.*, American Petroleum Institute, Washington, D.C.

Ashour, M., Norris, G. and Pilling, P. (1998), "Lateral loading of a pile in layered soil using the strain wedge model", *J. Geotech. Geoenviron.*, **124**(4), 303-315. https://doi.org/10.1061/(ASCE)1090-0241(1998)124:4(303).

Borja, R.I. and Amies, A.P. (1994), "Multiaxial cyclic plasticity model for clays", *Electron. J. Geotech. Eng.*, **120**(6), 1051-1070. https://doi.org/10.1061/(ASCE)0733-9410(1994)120:6(1051).

Bouzid, D., Bhattacharya, S. and Dash, S. (2013), "Winkler Springs (py curves) for pile design from stress-strain of soils: FE assessment of scaling coefficients using the Mobilized Strength Design concept", *Geomech. Eng.*, **5**(5), 379-399. http://doi.org/10.12989/gae.2013.5.5.379.

Brandenberg, S.J., Wilson, D.W. and Rashid, M.M. (2010), "Weighted residual numerical differentiation algorithm applied to experimental bending moment data", *J. Geotech. Geoenviron.*, **136**(6), 854-863. https://doi.org/10.1061/(ASCE)GT.1943-5606.0000277.

Brown, D.A., Morrison, C. and Reese, L.C. (1988), "Lateral load behavior of pile group in sand", *Electron. J. Geotech. Eng.*, **114**(11), 1261-1276. https://doi.org/10.1061/(ASCE)0733-9410(1988)114:11(1261).

Brown, D.A., Reese, L.C. and O'Neill, M.W. (1987), "Cyclic lateral loading of a large-scale pile group", *Electron. J. Geotech. Eng.*, **113**(11), 1326-1343.doi: https://doi.org/10.1061/(ASCE)0733-9410(1987)113:11(1326).

Brown, D.A. and Shie, C.-F. (1990), "Three dimensional finite element model of laterally loaded piles", *Comput. Geotech.*, **10**(1), 59-79. https://doi.org/10.1016/0266-352X(90)90008-J.

Chandrasekaran, S., Boominathan, A. and Dodagoudar, G. (2009), "Group interaction effects on laterally loaded piles in clay", *J. Geotech. Geoenviron.*, **136**(4), 573-582. https://doi.org/10.1061/(ASCE)GT.1943-5606.0000245.

Choi, J., Brandenberg, S.J. and Kim, M. (2013), "Modeling the dynamic behavior of a single pile in dry sand using a new py material model", *UCLA Previously Published Works, University of California, Los Angles.* https://escholarship.org/uc/item/1mg8x366.

Christensen, D.S. (2006), "Full scale static lateral load test of a 9 pile group in sand", Master's thesis, Brigham Young University,Provo,UT,USA.

Darendeli, M.B. (2001), "Development of a new family of normalized modulus reduction and material damping curves", Ph.D. dissertation, Univ. of Texas at Austin, Austin, Tex.

Fayyazi, M.S. (2015), *Numerical study on the response of pile groups under lateral loading*, Ph.D. Dissertation, University of British Columbia, Vancouver, British Columbia

Fayyazi, M.S., Taiebat, M. and Finn, W.L. (2014), "Group reduction factors for analysis of laterally loaded pile groups", *Can. Geotech. J.*, **51**(7), 758-769. https://doi.org/10.1139/cgj-2013-0202.

Ferritto, J.M. (1993), "Effects on high plasticity clay deposits on site ground amplification", *Proceedings of the International Conferences on Case Histories in Geotechnical Engineering*, St. Louis, Missouri.

Groholski, D.R., Hashash, Y.M., Kim, B., Musgrove, M., Harmon, J. and Stewart, J.P. (2016), "Simplified model for small-strain nonlinearity and strength in 1D seismic site response analysis", *J. Geotech. Geoenviron.*, **142**(9), 04016042. https://doi.org/10.1061/(ASCE)GT.1943-5606.0001496.

Kwak, D.Y., Brandenberg, S.J., Mikami, A. and Stewart, J.P. (2015), "Prediction equations for estimating shear-wave velocity from combined geotechnical and geomorphic indexes based on Japanese data set", *Seismol. Soc.*, **105**(4), 1919-1930. https://doi.org/10.1785/0120140326.

Larkela, A. (2008), "Modeling of a pile group under static lateral loading", Master's thesis, Helsinki University of Technology, Espoo,Finland.

Matlock, H. (1970), "Correlations for design of laterally loaded piles in soft clay", *Offshore technology in civil engineering's hall of fame papers from the early years.* 77-94.

Mayne, P.W. and Rix, G.J. (1995), "Correlations between shear wave velocity and cone tip resistance in natural clays", *Soils Found.*, **35**(2), 107-110. https://doi.org/10.3208/sandf1972.35.2_107.

McGann, C.R., Arduino, P. and Mackenzie-Helnwein, P. (2010), "Applicability of conventional py relations to the analysis of piles in laterally spreading soil", *J. Geotech. Geoenviron.*, **137**(6), 557-567. https://doi.org/10.1061/(ASCE)GT.1943-5606.0000468.

McVay, M., Casper, R. and Shang, T.I. (1995), "Lateral response of three-row groups in loose to dense sands at 3D and 5D pile spacing", *Electron. J. Geotech. Eng.*, **121**(5), 436-441. https://doi.org/10.1061/(ASCE)0733-9410(1995)121:5(436).

McVay, M., Zhang, L., Molnit, T. and Lai, P. (1998), "Centrifuge testing of large laterally loaded pile groups in sands", *J. Geotech. Geoenviron.*, **124**(10), 1016-1026. https://doi.org/10.1061/(ASCE)1090-0241(1998)124:10(1016).

Morrison, C.S. and Reese, L.C. (1988), *A Lateral-Load Test of a Full-Scale Pile Group in Sand*, TEXAS UNIV AT AUSTIN GEOTECHNICAL ENGINEERING CENTER

Muqtadir, A. and Desai, C.S. (1986), "Three-dimensional analysis of a pile-group foundation", *IJNAMG*. **10**(1), 41-58.doi: https://doi.org/10.1002/nag.1610100104.

Murchison, J.M. and O'Neill, M.W. (1984). "Evaluation of py relationships in cohesionless soils", *Analysis and Design of Pile Foundations*, 174-191.

Park, J.S., Park, D. and Yoo, J.K. (2016), "Vertical bearing capacity of bucket foundations in sand", *Ocean Eng.*, https://doi.org/10.1016/j.oceaneng.2016.05.056.

Poulos, H.G. and Davis, E.H. (1980), *Pile foundation analysis and design*, John Wiley and Sons, New York, N.Y.

Qin, H. and Guo, W.D. (2014), "Nonlinear response of laterally loaded rigid piles in sand", *Geomech. Eng.*, **7**(6), 679-703. http://doi.org/10.12989/gae.2014.7.6.679.

Rahmani, A., Taiebat, M., Finn, W.L. and Ventura, C.E. (2018), "Evaluation of py springs for nonlinear static and seismic soil-pile interaction analysis under lateral loading", *Soil Dyn. Earthq. Eng.*, **115** 438-447. https://doi.org/10.1016/j.soildyn.2018.07.049.

Reese, L., Wang, S., Arrellaga, J. and Hendrix, J. (1996), "Computer program GROUP for Windows, User's Manual, version 8.0", *Ensoft, Inc., Austin, Texas. 370.*

Reese, L.C., Cox, W.R. and Koop, F.D. (1974), "Analysis of laterally loaded piles in sand", *Offshore Technology in Civil Engineering Hall of Fame Papers from the Early Years*, 95-105.

Reese, L.C., Wang, S., Isenhower, W. and Arrellaga, J. (2004), "Computer program Lpile plus version 5.0 technical manual", *Ensoft: Austin, TX, USA*.

Rollins, K., Olsen, R., Egbert, J., Olsen, K., Jensen, D. and Garrett, B. (2003), *Response, analysis, and design of pile groups subjected to static & dynamic lateral loads*, Utah. Dept. of

Transportation. Research Division

Rollins, K.M., Lane, J.D. and Gerber, T.M. (2005), "Measured and computed lateral response of a pile group in sand", *J. Geotech. Geoenviron.*, **131**(1), 103-114. https://doi.org/10.1061/(ASCE)1090-0241(2005)131:1(103).

Rollins, K.M., Olsen, R.J., Egbert, J.J., Jensen, D.H., Olsen, K.G. and Garrett, B.H. (2006), "Pile spacing effects on lateral pile group behavior: load tests", *J. Geotech. Geoenviron.*, **132**(10), 1262-1271. https://doi.org/10.1061/(ASCE)1090-0241(2006)132:10(1262).

Rollins, K.M., Peterson, K.T. and Weaver, T.J. (1998), "Lateral load behavior of full-scale pile group in clay", *J. Geotech. Geoenviron.*, **124**(6), 468-478. https://doi.org/10.1061/(ASCE)1090-0241(1998)124:6(468).

Ruesta, P.F. and Townsend, F.C. (1997), "Evaluation of laterally loaded pile group at Roosevelt Bridge", *J. Geotech. Geoenviron.*, **123**(12), 1153-1161. https://doi.org/10.1061/(ASCE)1090-0241(1997)123:12(1153).

Sladen, J. (1992), "The adhesion factor: applications and limitations", *Can. Geotech. J.*, **29**(2), 322-326. https://doi.org/10.1139/t92-036.

Stacul, S., Squeglia, N. and Russo, G. (2020), "PRaFULL: A method for the analysis of piled raft foundation under lateral load", *Geomech. Eng*., **20**(5), 433-445. https://doi.org/10.12989/gae.2020.20.5.433.

Trochanis, A.M., Bielak, J. and Christiano, P. (1991), "Three-dimensional nonlinear study of piles", *Electron. J. Geotech. Eng.*, **117**(3), 429-447. https://doi.org/10.1061/(ASCE)0733-9410(1991)117:3(429).

Walsh, J.M. (2005), "Full-scale lateral load test of a 3x5 pile group in sand", Master's thesis, Brigham Young University, Provo, UT, USA.

Xu, C.J., Ding, H.B., Luo, W.J., Tong, L.H., Chen, Q.S. and Deng, J.L. (2020), "Experimental and numerical study on performance of long-short combined retaining piles", *Geomech. Eng*., **20**(3), 255-265. https://doi.org/10.12989/gae.2020.20.3.255.

Yang, Z. and Jeremić, B. (2002), "Numerical analysis of pile behaviour under lateral loads in layered elastic–plastic soils", *IJNAMG*, **26**(14), 1385-1406. https://doi.org/10.1002/nag.250.

Zhang, L., Silva, F. and Grismala, R. (2005), "Ultimate lateral resistance to piles in cohesionless soils", *J. Geotech. Geoenviron.*, **131**(1), 78-83. https://doi.org/10.1061/(ASCE)1090-0241(2005)131:1(78).

Zhang, W., Esmaeilzadeh Seylabi, E. and Taciroglu, E. (2017), "Validation of a three-dimensional constitutive model for nonlinear site response and soil-structure interaction analyses using centrifuge test data", *IJNAMG*, **41**(18), 1828-1847. https://doi.org/10.1002/nag.2702.

GC